

Computational determination of effective properties of rocks using 3D tomographic images

Erik H. Saenger*, ETH Zurich and Spectraseis, Frieder Enzmann, Universität Mainz, Youngseuk. Keehm, Kongju National University.

Summary

This paper is concerned with numerical considerations of effective transport and effective mechanical properties of rocks. We derive these properties directly from rock microstructure using 3D tomographic images. Permeability values were estimated through Lattice-Boltzmann (LB) flow simulations. The effective shear and P-wave modulus is derived by dynamic wave propagation simulations. We apply a displacement-stress rotated staggered finite-difference (FD) grid technique to solve the elastodynamic wave equation. An accurate approximation of a Newtonian fluid is implemented in this technique by using a generalized Maxwell body. We give a practical description how to use this approach. An additional accuracy condition for simulations with viscous fluid infill is described. This condition requires that the spatial grid size is several times smaller than the thickness of the dynamic viscous boundary layer adjacent to the fluid/solid interface.

Introduction

Digital rock methodology combines modern microscopic imaging with advanced numerical simulations of the physical properties of rocks. Modeling of elastic-wave propagation directly from rock microstructure is integral to this technology. Additionally we determine the permeability of the digitized rock samples. Our computer simulations provide a combined estimate of transport and mechanical properties of exact the same structure.

In this paper we describe our approach for one digitized rock sample of sandstone. We concentrate on a detailed description how to use the rotated staggered grid (RSG) finite-difference (FD) method for pore-scale simulation of elastic wave propagation in digital rock samples, including the dynamic elastic properties of rocks saturated with a viscous fluid. It is planned to apply our methodology to samples of gas hydrate bearing sediments (e.g. Murshed et al. 2008).

Digital Rock Sample

Synchrotron-based X-ray tomographic microscopy (XTM) is suitable to provide data on the real pore microstructure of rocks. In Figure 1 we illustrate our final digitized model after several processing steps. It contains 3 different phases: grain material (invisible), pore geometry (grey) and oil bubbles (blue). The pores are 100% connected. The distribution of the oil blobs is derived with numerical flow simulations and is not a direct result of the tomography.

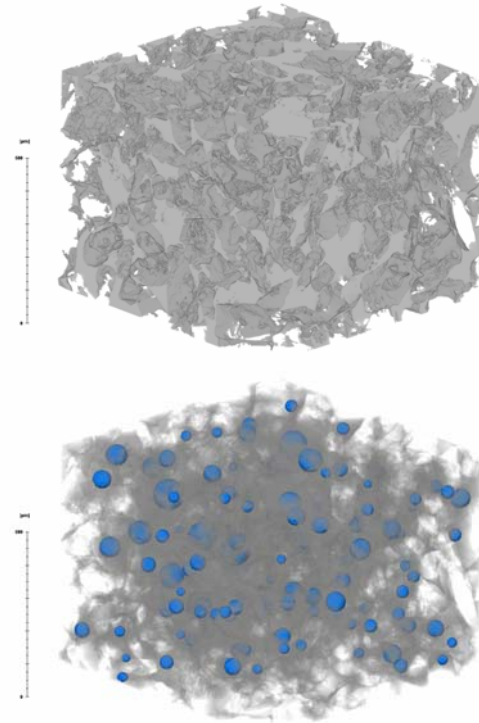


Figure 1: Digitized rock sample used in this paper. The pore structure (top) is illustrated in grey. The size of the model is $302 \times 400 \times 400$ gridpoints with a resolution of $2.275 \mu\text{m}$. The blue bubbles show the distribution of oil (bottom). The porosity is $\phi=0.24$, the water saturation is $S_w=0.98$ and the oil saturation is $S_o=0.02$.

Permeability

Permeability is estimated by conducting numerical flow simulations on the 3D digital rock, using the lattice-Boltzmann (LB) method (Keehm et al., 2004). The LB method is a robust technique that simulates fluid flow according to simple rules governing local interactions between individual particles (Doolen, 1990) and recovers the Navier-Stokes equations at the macroscopic scale (Ladd, 1994). Prime advantages of the LB method are its ability to handle any discrete geometry without simplification and its accuracy in describing flow through porous media (Keehm et al., 2001 & 2006). Artifacts can occur in the local velocity fields (Manwart et al., 2002), but applying time-averaged velocities mitigates these effects (Ladd, 1994). The numerical flow simulation was

Computational Rock Physics

performed with an assigned pressure gradient (∇P) across opposite faces of cubical digital rocks. We imposed no-flow boundary condition on the other four side faces of the cube. From the simulated local flux field, we calculated a volume-averaged flux $\langle q \rangle$. Then, the macroscopic permeability κ was estimated using the Darcy's law:

$$\langle q \rangle = \frac{\kappa}{\eta} \nabla P \quad (1)$$

where η is the dynamic viscosity of the fluid. We repeated the LB simulation with 1-D pressure gradient for all three directions and the permeability was estimated by three permeability values (κ_x , κ_y and κ_z). The local velocity fields from three different simulations are shown in Figure ?? and permeability values can be found in Table ?. With the permeability it is possible to calculate the Biot reference frequency.

In the future, we plan to apply two-phase LB flow simulations on the digital rocks (Keehm, 2003). The results of two-phase flow simulations will give the detailed distribution of two fluids in the pore geometry that can be used for accurate elastic property prediction, as well as the estimation of relative permeability.

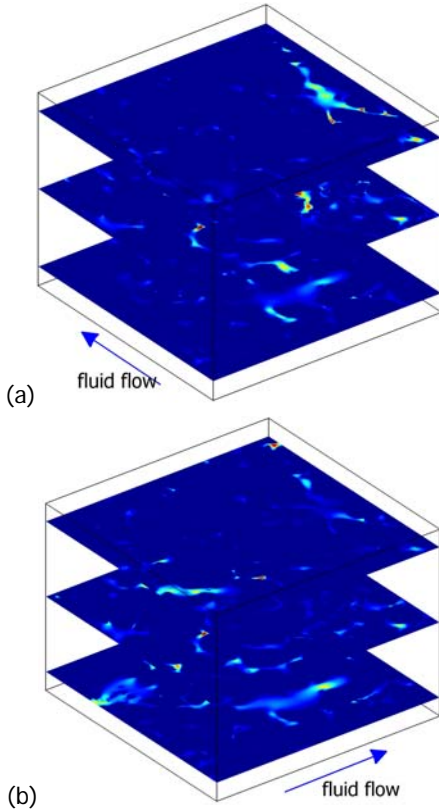


Figure 2: Local velocity distributions from the LB flow simulations. Diagrams show normalized local velocity values by 1-D pressure gradients of (a) X-, (b) Y- and (c) Z-direction.

Wave Propagation Modeling Procedure

We apply the 3D RSG-technique with the viscoelastic extension described in Saenger et al. (2005) to explicitly model wave propagation in fluid saturated porous media. The synthetic porous rock-models are embedded in a homogeneous elastic region. The full models are made up of $804 \times 400 \times 400$ grid points with an interval of $\Delta x = 0.0005$ m. The interval with the structure shown in Figure 1 is in the center of the full model. In the homogeneous region and for the grain material we set a P -wave velocity of $v_p = 5100$ m/s, a S -wave velocity of $v_s = 2944$ m/s and a density of $\rho_{\text{grain}} = 2540$ kg/m³. For dry pores we set $v_p = 0$ m/s, $v_s = 0$ m/s and $\rho = 0.0001$ kg/m³; for water-saturated (non-viscous) pores we use $v_p = 1485$ m/s, $v_s = 0$ m/s and $\rho = 1000$ kg/m³. For the pores filled with a viscous fluid we use the parameters given in the next section. We perform our modeling experiments with periodic boundary conditions in the two horizontal directions.

The source wavelet is the first derivative of a Gaussian with a dominant frequency of $f_{\text{source}} = 2 \times 10^5$ Hz and with a time increment of $\Delta t = 2.1 \times 10^{-9}$ s. All computations are performed with second order spatial FD operators and with a second order time update. A similar numerical setup with a detailed error analysis is discussed by Saenger et al. (2005).

Viscous Pore Infill

In this section we give a practical description how to numerical implement viscous pore infill by using the technique described in Saenger et al (2005). It is based on the viscoelastic formulation of Emmerich and Korn (1987)

Computational Rock Physics

and Kristek and Moczo (2003). For one fluid with a specific viscosity η we use one relaxation mechanism.

First step is to set the high-frequency limit of the shear wave modulus c_{44} . The stability criterion of the used FD technique have to be fulfilled (Eq. 12 of Saenger et al. 2005). However, from a practical point of view the following rule of thumb can be applied:

$$c_{44} = \tau \times v_p^2 \times \rho_{fluid} \quad (2)$$

with v_p as the P -wave in the fluid at a frequency of 0 Hz and ρ_{fluid} as the density of the viscous fluid. The factor τ is chosen here to be 50.

The high frequency limit of the P -wave modulus is calculated with Eq. 10 of Saenger et. al (2005):

$$c_{11} = \lambda(0) + 3c_{44} \quad (3)$$

with $\lambda(0) = v_p^2 \times \rho_{fluid}$.

The two independent anelastic coefficients \tilde{Y}_1^{44} and \tilde{Y}_1^{11} are set to (derived from Eq. 4 of Saenger et al. 2005):

$$\tilde{Y}_1^{44} = c_{44}; \quad (4)$$

$$\tilde{Y}_1^{11} = c_{11} - \lambda(0). \quad (5)$$

The viscosity η of the fluid can be varied by the variation of the angular relaxation frequency ω_1 (Eq. 8 of Saenger et al. 2005):

$$\eta = \frac{c_{44}}{\omega_1}. \quad (6)$$

The viscosity is modeled accurately if (Saenger et al. 2005):

$$2\pi f_{source} \ll \omega_1 \quad (7)$$

For our example we calculate our modeling parameters with Eq.(2-5) by using $v_p=1500$ m/s, $\rho_{fluid} = 800$ kg/m³ and $\omega_1=1 \times 10^8$ Hz. The resulting viscosity is 900 Pa s.

Discretization of Viscous Skin Depth

Ciz et al. (2006) perform numerical simulations for a system of alternating elastic solid and viscous fluid layers. Such a system is known to exhibit many features of the poroelastic medium. This idealized system is used for numerical modeling of elastic wave dispersion and attenuation to test the precision of the extended viscous version of the RSG. They obtain very good agreement between the numerical simulations and the analytical solution for a wide range of viscosities, but observe significant discrepancies at low viscosities. These discrepancies cannot be attributed to numerical dispersion. Their analysis shows that discrepancies at low viscosities may be caused by insufficient sampling of the viscous boundary layer near the solid/fluid interface. They find that

it is necessary to properly discretize the viscous skin depth $\delta = (2\eta / (2\pi f_{source} \rho_{fluid}))^{1/2}$ (defined by the lefthand side of Eq. 8). The viscous boundary layer plays an important role when modeling elastic wave propagation in the medium containing viscous fluids. The accuracy of the numerical results is sufficient, if the skin depth is discretized with at least three gridpoints:

$$\delta = (2\eta / (2\pi f_{source} \rho_{fluid}))^{1/2} \geq \xi \Delta x, \xi \approx 3 \quad (8)$$

where ρ_{fluid} is the fluid density, η denotes viscosity, f_{source} is the frequency of the propagation wave, and Δx represents the spatial step. In addition to the standard stability criterion and the standard numerical dispersion condition the inequality in Eq. 8 should be regarded as a third accuracy condition, necessary for modeling elastic-wave propagation on micro-scale in the presence of viscosity. With our modeling parameters described above we fulfill this accuracy condition.

Effective Properties of the Digitized Rock Sample

To obtain effective velocities in different models we apply a body force plane source at the top of the model. The plane P - or S -wave generated in this way propagates through the porous medium. Figure 2 illustrates a slice of a snapshot of the wavefield. We measure the time-delay of the peak amplitude of the mean plane wave caused by the inhomogeneous region. Using the time-delay we estimate the effective velocity and, therefore, also the corresponding elastic moduli. In Table 1 we summarize our results for the effective properties of our considered digitized rock shown in Figure 1.

Computational Rock Physics

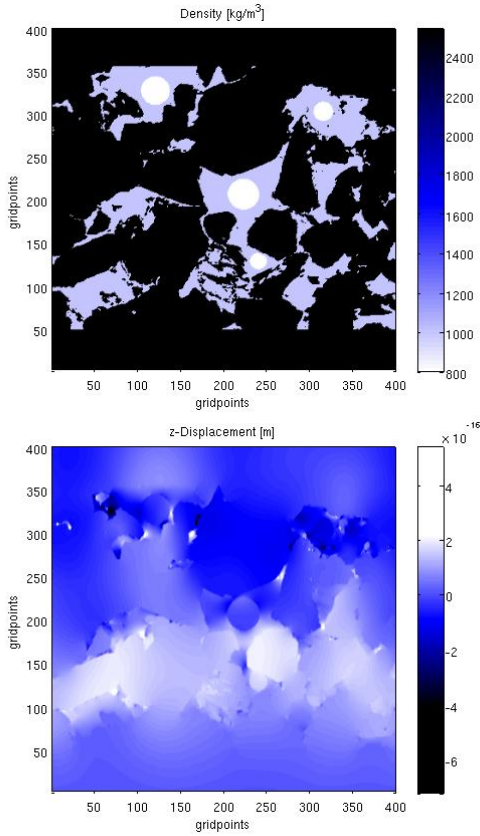


Figure 3: Top: Slice of the density of the model shown in Figure 1. Bottom: A slice (same position as the density slice) of the 3D z-displacement field after several timesteps.

Size	400 * 400 * 308
Porosity ϕ	0.242165
Grid spacing	2.275 μm
Perm. x-direction (mD)	945.3
Perm. y-direction (mD)	991.7
Perm. z-direction (mD)	1066.0
Normalized effective P-wave modulus ($\langle C_{11} \rangle / C_{11\text{grain}}$)	0.482
Normalized effective shear modulus ($\langle C_{44} \rangle / C_{44\text{grain}}$)	0.496

Table 1: Effective properties of the digitized rock sample. Effective transport and effective mechanical properties are derived for the digitized rock model shown in Figure 1.

Conclusions

In this paper we describe numerical estimations of effective properties of a rock using a 3D tomographic image. We perform finite-difference simulations on the micro-scale to determine effective elastic properties including viscous Biot-coupling. We describe how to use a generalized Maxwell body (Emmerich and Korn, 1987; Kristek and Moczo, 2003) and a displacement-stress rotated staggered grid scheme to simulate wave propagation in a heterogeneous rock sample. Using this technique it is possible to saturate digitized rock models with a realistic approximation of a Newtonian fluid (i.e. viscous oil). This allows us to study coupling mechanism of fluid-solid interaction which are covered by the elastodynamic wave equation. We point out the importance of an additional accuracy condition for simulations with viscous fluid infill. This condition requires that the spatial grid size be several times smaller than the thickness of the dynamic viscous boundary layer adjacent to the fluid/solid interface. Additionally, we determine the effective permeability using Lattice-Boltzmann (LB) flow simulations. This gives us the possibility to compare mechanical and transport properties derived for exact the same digital rock samples.

Acknowledgments

E. H. Saenger thanks the DFG (Deutsche Forschungsgemeinschaft) for supporting him through a Heisenberg scholarship (SA 996/1-1).